Optical characterization of the evolution of ion-induced anisotropic nanopatterns on Ag(001)

Frank Everts, Herbert Wormeester, and Bene Poelsema
MESA+ Research Institute, University of Twente, P.O. Box 217, NL-7500 AE Enschede, The Netherlands
(Received 9 September 2010; revised manuscript received 9 June 2011; published 15 July 2011)

Reflection anisotropy spectroscopy is used as an *in situ* probe for the emergence and evolution of surface patterns on Ag(001) during oblique incidence ion bombardment. The information is extracted from plasmon resonances induced by the nanoscale patterns, utilizing the fact that smooth Ag(001) is optically isotropic. The Rayleigh-Rice perturbation approach delivers the temporal development of the average periodicity and amplitude of the surface patterns. For ion bombardment at a polar angle of incidence of 70° along a ⟨110⟩ azimuth, strongly anisotropic surface features develop, giving rise to a single plasmon resonance, which is described well with a one-dimensional power spectral density function. For a smaller polar angle of incidence of 61.5° multiple plasmon resonances are observed, which demand a two-dimensional power spectral density function for a perfect description. These result compare well with high-resolution low-energy electron diffraction data, taken after ion bombardment at both angles of incidence. The optical data, obtained at 61.5°, show coarsening and seem to suggest scaling of the periodicity and roughness, with critical exponents 0.27 and 0.40, respectively.

DOI: 10.1103/PhysRevB.84.035403 PACS number(s): 79.20.Rf, 81.16.Rf, 61.05.jh, 73.20.Mf

I. INTRODUCTION

Ion bombardment of surfaces can be used to both smooth and roughen surfaces. The bombardment process can be such that an erosion instability is induced, leading to the formation of a variety of nanopatterns including ripples and dots.[1–5] The key parameter to characterize the nanopattern is its average lateral periodicity. Also the height variation, or roughness, and the distribution of the lateral periodicity are important quantities that characterize the nanopattern. The temporal evolution of these statistical quantities is an essential ingredient for understanding the mechanisms involved in the self-organization process.[6] This temporal evolution is most effectively studied with techniques that can be employed *in situ*. Both x-ray scattering[7] and light scattering[8,9] have been used to characterize *in situ* the evolution of ion-induced ripple patterns. However, not only the scattered beam, but also a specularly reflected light beam contains a wealth of information about the periodicity and shape of structures. We demonstrated this by monitoring the evolution of ripple patterns created by means of glancing incidence ion bombardment of a Ag(001) surface via the variation of the specular optical reflection.[10] The coupling between the periodicity of structures and the resonance energy of generated surface plasmons enables a quantitative analysis.[11,12]

The cubic symmetry of the Ag(001) gives rise to an isotropic optical response. An anisotropic pattern that evolves during oblique incidence ion sputtering results in an easily identifiable anisotropic optical response. This optical anisotropy can be measured with reflection anisotropy spectroscopy (RAS). This technique involves a normalized optical bridge setup that allows a sensitive measurement of the difference in reflectivity r along two orthogonal directions ($r_\perp$ and $r_\parallel$) on the surface:[13]

$$\frac{\Delta r}{r} = 2\frac{r_\perp - r_\parallel}{r_\perp + r_\parallel}. \quad (1)$$

The high sensitivity of RAS for recording optical anisotropy has led to its use to monitor semiconductor growth,[14] to probe surface electronic states,[15] to measure morphological surface structures (i.e., steps and islands),[16] and to determine the orientation and crystalline properties of adsorbed organic molecules.[17] For a few deposited metal particle systems the plasmon resonance feature was studied with RAS.[18–20] The virtue of RAS in the study of nanopattern evolution during ion bombardment is that all isotropic contributions are suppressed. The focus is on the anisotropic contribution, i.e., the periodicity and the modulation height of the ion-induced anisotropic pattern. The sign of the anisotropy signal already reveals the direction along which the periodicity evolves. For ripple structures, the spectra will only show plasmon-induced features with the same sign. In this paper we report on the observation of unique features with opposite sign in the optical anisotropy spectra. These features reflect the organization of etch pit structures not only perpendicular to, but also parallel to the plane of incidence of the ion beam. The average shapes of the etch pit structures are elucidated from electron diffraction.

II. EXPERIMENTAL DETAILS

The experimental data were obtained during ion beam erosion experiments performed on a single-crystalline Ag(001) sample in a UHV system. The sample was cleaned with multiple ion bombardment and anneal cycles. For the RAS measurements, a home-built system was used,[10] the performance of which is analogous to instruments described in literature.[13,14] The measurements described in this paper reflect the real part of the optical anisotropy given in Eq. (1). The photomultiplier amplification was regulated to provide a constant dc reflectivity signal. This regulated photomultiplier voltage is used in the fit procedures as a measure of the accuracy of the experimental data. The light is incident along the normal of the surface. The parallel polarization direction in the optical experiments is aligned with respect to the plane of incidence of the ion beam. The measured anisotropy is the normalized difference between the two directions parallel and perpendicular to the plane of incidence of the ion beam. High-resolution low-energy electron diffraction (HR-LEED) measurements with an Omicron SPA-LEED instrument were

used to characterize the average morphology of the periodic structures on the surface.

III. ANISOTROPIC OPTICAL RESPONSE OF NANOSTRUCTURED SURFACES

The ability to incorporate the influence of roughness on optical spectra was given a firm base by the work of Aspnes and co-workers.[21] Later studies provided a comparison of the roughness value obtained from Atomic Force Microscopy (AFM) and ellipsometry.[22] A clear one-to-one relation between the two was observed, albeit the actual value derived from ellipsometry differed. Recently, Sperling and Abelson[23] showed by comparing AFM and ellipsometric measurements on deposited hydrogenated silicon films that it is not just the rms roughness but also the lateral length scale that influences the optical signal. The traditional effective-medium approach used to model roughness fails to incorporate this effect. Sperling and Abelson[23] conclude "that a more complicated theory" is required to address the effect of the lateral length scale. For this they use the Rayleigh-Rice theory, a perturbation of the solution of the Maxwell equations. With this, they showed that for a characteristic length scale much smaller than the wavelength of the light used, the effect of rms roughness and lateral length scale cannot be separated. The Rayleigh-Rice perturbation was also required by Kretschmann and Kröger to understand the influence of surface roughness on a silver surface on the optical response.[11] The Rayleigh-Rice approach provides the correct spectral shape of the characteristic plasmon resonance. However, it can also be used to model features with a lateral length scale of the order of the wavelength of light. In this length scale range, the plasmon resonance energy depends on the actual length scale, a phenomenon widely used in plasmonics to couple light in a diffraction grating.[12] For the analysis of our RAS spectra we use a more generalized description of Rayleigh-Rice that was derived by Franta and Ohlidal.[24] The perturbation of the solution of the Maxwell equations for a sharp interface expresses the change of the reflectivity as

$$\hat{r}_{\perp,\parallel} = \hat{r}^{(0)}_{\perp,\parallel} + \sigma^2 \int_{-\infty}^{\infty}\int_{-\infty}^{\infty} \hat{f}_{\perp,\parallel}(\vec{K},k_0) \times w(\vec{K}) d\vec{K}, \quad (2)$$

where $\hat{r}^{(0)}_{\perp,\parallel}$ is the reflectivity of the unperturbed surface. The surface roughness is quantified by the rms roughness σ and the normalized power spectral density function (PSDF) $w(\vec{K})$. This spatial information is spanned by the spatial wave vector $\vec{K}$ on the surface. The interaction with the light is provided by the kernel $\hat{f}$, which depends on the wave vector of the incident light k_0 and the reciprocal length $\vec{K}$. For normal incidence, the kernel $\hat{f}_\perp$ can be written as

$$\hat{f}_\perp(K_\parallel) = -2k_0\hat{r}^{(0)}_\perp|\hat{K}|\left(\frac{k_0}{|\hat{K}|}\sqrt{\epsilon} + \frac{(\hat{b}-\hat{c})\left[\left(\frac{K_\parallel}{K}\right)^2 + \hat{b}\hat{c}\right]}{1+\hat{b}\hat{c}}\right), \quad (3)$$

with $\hat{b}$, $\hat{c}$, and K defined as

$$\hat{b} = \sqrt{\left(\frac{k_0}{K}\right)^2 - 1},$$
$$\hat{c} = \sqrt{\left(\frac{k_0}{K}\right)^2 \epsilon - 1}, \quad (4)$$
$$K = \sqrt{K_\perp^2 + K_\parallel^2} = |\vec{K}|.$$

The dielectric constant of the reflecting material is expressed by ϵ. For $\hat{f}_\parallel$ an analogous expression is found. Note that Eq. (3) seems to indicate that the reflectivity in one direction depends only on the spatial wave vector in the orthogonal direction. This is true only at first glance, as the coefficients $\hat{b}$ and $\hat{c}$ also depend on the magnitude of the spatial wave vector.

With these definitions the reflectivity difference of an anisotropically rough surface on top of an optically isotropic substrate can be evaluated:

$$\frac{\Delta r}{r} = 2\frac{(r_\perp - r_\parallel)}{(r_\perp + r_\parallel)} = \frac{\sigma^2}{\hat{r}^{(0)}}\int_{-\infty}^{\infty}\int_{-\infty}^{\infty}(\hat{f}_\perp - \hat{f}_\parallel) w(\vec{K}) d\vec{(K)}, \quad (5)$$

where $\hat{r}^{(0)} = \frac{1}{2}(\hat{r}^{(0)}_\perp + \hat{r}^{(0)}_\parallel)$. The difference in the kernel $\hat{f}$ reduces to

$$\hat{f}_\perp - \hat{f}_\parallel = -2k_0\hat{r}^{(0)}|\vec{K}|\frac{(\hat{b}-\hat{c})\left[\left(\frac{K_\parallel}{K}\right)^2 - \left(\frac{K_\perp}{K}\right)^2\right]}{(1+\hat{b}\hat{c})} = -2k_0\hat{r}^{(0)}|K|\frac{(\hat{b}-\hat{c})}{(1+\hat{b}\hat{c})}\cos 2\phi. \quad (6)$$

The angle ϕ represents the direction of $\vec{K}$ with respect to the parallel direction. The anisotropic response measured with RAS is related to the surface roughness by

$$\frac{\Delta r}{r} = -2k_0\sigma^2\int_{-\infty}^{\infty}\int_{-\infty}^{\infty}\frac{(\hat{b}-\hat{c})}{(1+\hat{b}\hat{c})}|K|w(\vec{K})\cos 2\phi d\vec{(K)}. \quad (7)$$

The anisotropic part of the roughness contribution that is measured with RAS is selected by the $\cos 2\phi$ term. The optical response of a grating can be simulated using Eq. (7).[10] Figure 1 shows the relation between the lateral length scale and the plasmon resonance energy position. This result of the Rayleigh-Rice calculation is compared to the well-known plasmon dispersion equation (see, for example, Ref. 12). This dispersion relation is widely used to find the combination of the optical wavelength and grating period for efficient plasmon coupling in a grating. Slight deviations between the RRT and plasmon dispersion formula occur as a result of the finite distribution of the grating period used in the simulations. The determination of the plasmon resonance is thus a direct measure of the lateral length scale. This figure also shows that below a lateral length scale of 100 nm, the resonance energy position is constant at 3.7 eV, i.e., the photon energy at which the real part of the dielectric function of silver is -1. This has a direct consequence for the ability to distinguish between lateral length scale and rms roughness. In this lateral length

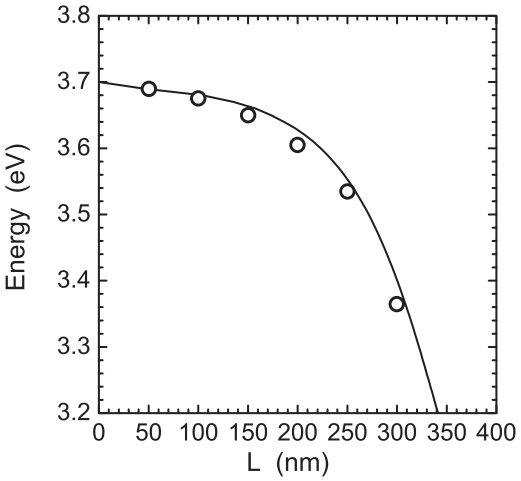

FIG. 1. Relation between periodicity and resonance energy obtained from a simulation of a 1D grating (○) and from the plasmon dispersion relation (Ref. 12).

scale regime, the conclusion of Sperling and Abelson[23] applies that these two parameters cannot be independently determined from optical spectroscopy and thus hinders the study of kinetic roughening with ellipsometry. The effect of roughness in this case can be modeled by the Aspnes approach,[21] i.e., a thin layer which has an effective thickness and an effective dielectric function. The effective thickness is determined by both the actual rms and the lateral length scale, while the dispersion of the effective dielectric function does not depend on these parameters. A change in resonance energy clearly signifies that effective dielectric function is also effected and the Aspnes approach is no longer feasible. Therefore, Fig. 1 shows that a lower limit of ∼100 nm has to be observed for the distinction between lateral periodicity and rms roughness. A resonance energy position that differs from 3.7 eV allows to separately determine rms roughness and lateral length scale from the optical spectrum.

IV. RAS MEASUREMENTS

Figures 2(a) and 2(b) display the development of the RAS signal for sputtering with 2-keV Ar^+ ions at a polar angle of incidence of 70° along the [110] azimuth at a surface temperature of 350 and 300 K, respectively. An ion current of 5 μA/cm^2 recorded for normal incidence sputtering was used. The top part shows the anisotropy spectrum as recorded at the end of the measurement. The high-temperature measurement [Fig. 2(a)] shows that the evolution of the plasmon resonance is characterized by an increase of the resonance strength and strength combined with a redshift of the resonance energy with fluence. The negative sign of the RAS feature indicates that the etch pits show a periodicity in the direction perpendicular to the plane of the incident ion beam. This periodicity reveals the evolution of ripple structures parallel to the plane of incidence.[25,26] These spectra can be described well with a (semi-) one-dimensional (1D) surface morphology modulation.[10] The observed redshift indicates that the length scale of the periodicity is just above 200 nm after 1000 min of ion erosion. Initially the resonance energy is just below 3.7 eV,

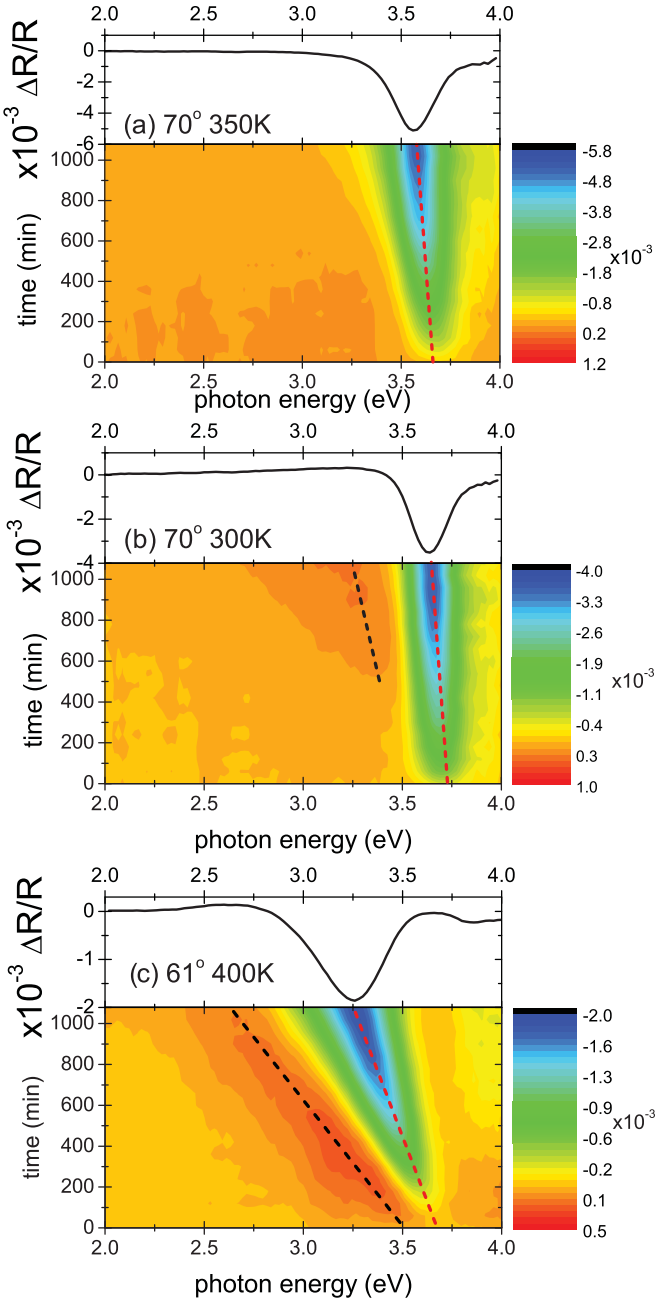

FIG. 2. (Color online) RAS measurement as a function of sputter time. The incident 2-keV Ar^+ ion beam had an ion current of 5 μA/cm^2 at normal incidence. The images show three different temperature and polar angle of incidence conditions: (a) 350 K, 70°, (b) 300 K, 70°, and (c) 400 K 61.5°. The red dashed line is a guide to the eye for the negative maximum, while the black dashed line is a guide to the eye for the observation of a positive maximum. The displayed spectra are the last spectra measured in the three time series.

indicating a length scale ∼50 nm or smaller. This value in the initial regime corresponds well with the scanning tunneling microscopy (STM) image at this temperature recorded by Valbusa *et al.* after 20 min of a Ne ion bombardment at 1 keV.[2] Note that the sputter conditions, i.e., fluence, ion type, and ion energy, differ. This limits the comparability of the results. Although the spectra recorded at 300 K [Fig. 2(b)] look similar

to those recorded at 350 K, they also show a slight, broad positive feature at ∼3.0–3.5 eV, which can be distinguished after ∼500 min of sputtering. The maximum of this positive feature is indicated with the black dashed line. It indicates that also a slight ordering of the individual etch pits occurs in the direction parallel to the plane of incidence of the ion beam. The resonance energy of the negative peak in the 300 K measurement is at a slightly higher energy than in the 350 K. This indicates that the periodicity of the main structure is smaller in the low-temperature situation. This is a direct result of the lesser diffusion of species at a lower temperature.[2,26] The positive resonance shows a considerably larger redshift with sputter time than the negative feature. Simulations show that this larger shift reflects the increased sensitivity for the characteristic length scale in this part of the spectrum.[27]

The ordering of etch pits parallel to the plane of incidence of the ion beam, as evidenced by the positive optical feature, can be influenced by the angle of incidence of the ion beam. Figure 2(c) shows the result for a polar angle of incidence of 61.5°. Note that this change in the polar angle of incidence also influences the ion flux; the flux at 61.5° is 40% higher than at 70°. The increased flux with decreasing polar angle of incidence would lead to an increased number of diffusing species on the surface. This would result in a decreased length scale. To compensate for this effect, the sample temperature is increased to 400 K to assure sufficient diffusion on the surface and thus the emergence of a characteristic length scale above 200 nm. The displayed evolution shows two well-pronounced features of opposite sign, indicating the orientation of etch features with two distinctly different, orthogonally oriented, length scales. Both resonances show a distinct redshift, revealing a considerable increase in average periodicity (coarsening) with sputter time.

V. LEED MEASUREMENTS

To elucidate the average shape of the etch features, LEED images were taken after sputtering of the Ag(001) surface. Such images as displayed in Fig. 3 show that markedly different structures evolve during sputtering at a polar angles of 70° and 61.5°. The images recorded for the more oblique incident angle were related to an etch pit with a top view of a slightly distorted rhombus shape and facets with an inclination angle ∼23°.[10] This average etch pit structure was evaluated from the electron energy dependency of the four observed diffraction features. Variation of the electron energy and the corresponding position change of the diffraction feature are used to evaluate the normalized parallel ($\vec{q}$) and perpendicular scattering vector ($S_{[001]}$).[28] The normalization is with respect to the reciprocal lattice vectors of Ag(001). The electron energy dependency of the four diffraction features recorded after sputtering at an angle of 61.5° is displayed in Fig. 4. This image shows that the position of the diffraction features in the Brillouin zone is electron energy dependent and moves to a single spot for the in-phase condition ($S_{[001]} = 5$). This indicates that these diffraction features signify the presence of facets. The orientation of these facets is derived from the slope seen in the $S_{[001]}$-$\vec{q}$ plot (see, e.g., Ref. 29 and references therein). The facet on the illuminated side shows an inclination angle of 13.6°, while the others show an inclination angle of

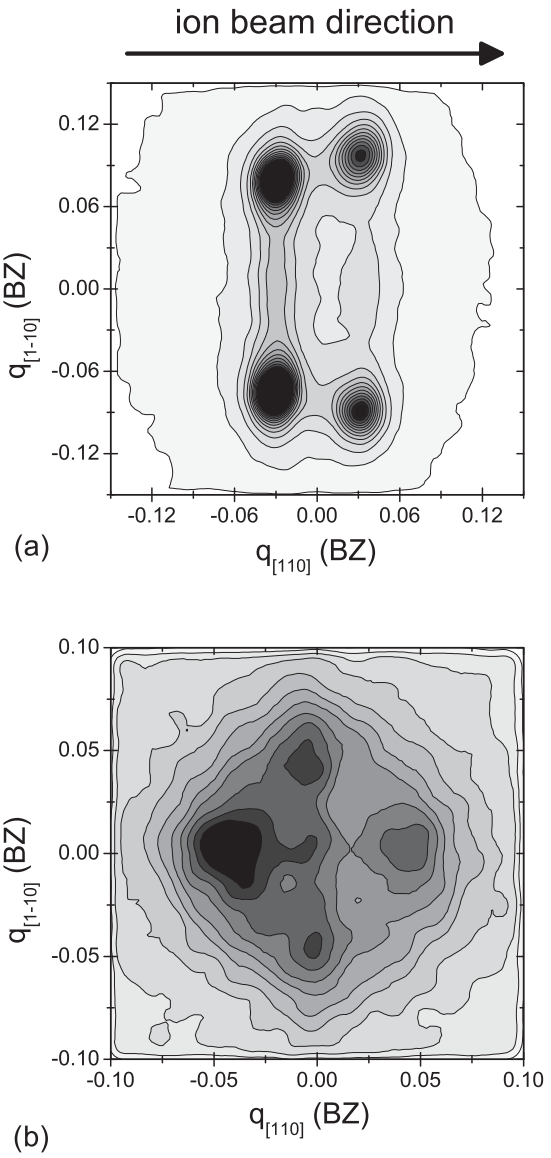

FIG. 3. HR-LEED pattern measured after ion bombardment of the Ag(001) surface as displayed in Figs. 2(a) and 2(c). (a) Polar angle 70° and temperature 350 K, measured at an electron energy of 210.7 eV ($S_{[001]} = 4.806$) and (b) polar angle 61.5° and 400 K, measured at an electron energy of 216.0 eV ($S_{[001]} = 4.866$).

∼17°. These angles indicate facet orientations around [117] and [115], respectively. The intensity and the different angle on the illuminated side is explained by the local angle of incidence on this facet. For the polar angle of incidence used, the local angle of incidence is 15°, just around the critical sputter angle.[30] This leads to a different sputter condition, resulting in the altered illumination. From the combination of the RAS and LEED measurements, we conclude that the average shape of the etch pits is an inverse mound with rectangular base. The rectangular structure is retrieved from the RAS measurements that provide the periodicity in both directions.

The very different diffraction patterns observed for sputtering at a polar angles of incidence of 70° and 61.5° were already indicative for the different average etch pits, i.e., a rhombus and an inverse rectangular mound, respectively. Such

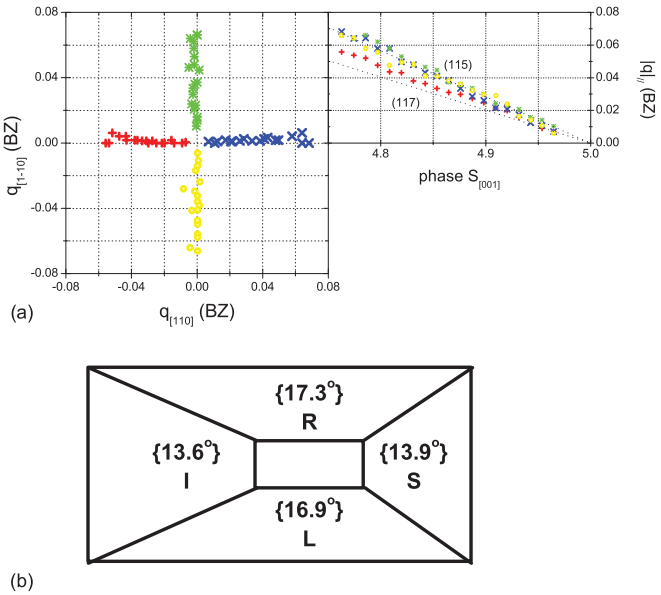

FIG. 4. (Color online) Position of the facet spots measured as a function of the electron energy for the pattern as displayed in Fig. 3(b). (a) Left-hand panel: The four facet peak positions as a function of the parallel scattering vector of the electron beam $\vec{q}_{\parallel}$. The value of $\vec{q}_{\parallel}$ in the $[1\bar{1}0]$ and [110] azimuth is plotted for electron energies between 203.1 and 223.2 eV. Right-hand panel: The average parallel components of the scattering vector change for the various facets vs the vertical scattering phase $S_{[001]}$. The surface component of the ions is parallel to the $[1\bar{1}0]$. (b) Sketch of the average etch pit shape with the four facet angles indicated. The ion beam is incident from the left. I indicates the illuminated facet and S indicates the shadowed facet. R and L indicate both right and left sides.

a strong angular dependence was also observed for the very similar Cu(001) surface.[26] Two key factors strongly influence these structures. The first one is the interlayer mass transport, which is on this surface determined by the Ehrlich-Schwoebel barriers. These barriers are very different for the ⟨110⟩ and ⟨100⟩ step edges on this surface.[26,31–33] Second, the result of the ion impact shows a strong dependence on the crystal structure observed at angles of incidence near the critical angle for channeling.[34]

VI. DETERMINATION OF ROUGHNESS EVOLUTION

The RAS spectra recorded during ion beam sputtering at 70° shown in Fig. 2(a) show a strong feature with a negative sign. This signals an anisotropy with a periodicity in only one direction, perpendicular to the ions' plane of incidence. This roughness can be described well with a single 1D Gaussian PSDF[10]

$$w(\vec{K}) = \frac{\sigma^2}{\sqrt{2\pi}\,\delta} e^{-(\vec{K}-\vec{K}_0)^2/2\delta^2}, \tag{8}$$

with K_0 the average reciprocal length, δ the width of the distribution, and σ the rms of the anisotropic part of the surface roughness. The actual PSDF characteristic for the roughness consists in this case of an azimuthally isotropic and an anisotropic component in the direction perpendicular to the ion beam. The RAS measurements are not sensitive to the

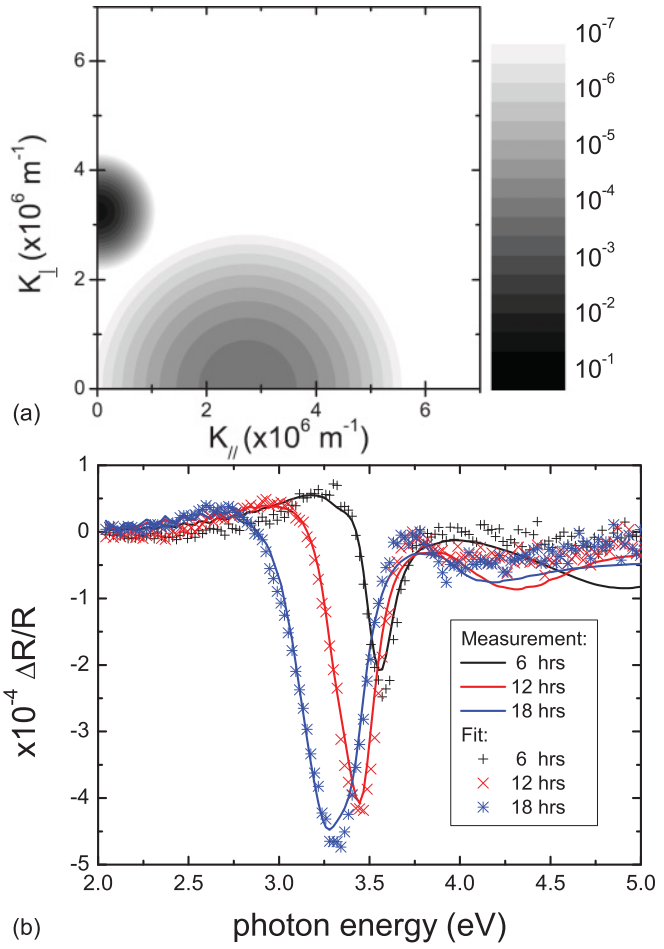

FIG. 5. (Color online) (a) Contour plot of the anisotropic PSDF obtained from a fit to the RAS spectrum recorded after 18 h sputtering at a polar angle of 61.5°. (b) Measured and fitted results at three stages of the ion sputtering at a polar angle of 61.5°.

first, and only the anisotropic part is probed. Different model functions for the anisotropic roughness distribution were investigated. The single Gaussian function characterized by three fit parameters (σ, δ, and $\vec{K}_0$) gave the best representation of the measured data with a limited number of coefficients.

The RAS spectra obtained for an incident angle of the ion beam of 61.5° are more complicated. The positive and negative peaks reflect a significant deviation from the isotropic roughness PSDF in, respectively, both the perpendicular and parallel direction. This anisotropy was modeled with two Gaussians to represent the observed periodicity in both the parallel and perpendicular direction:

$$w(\vec{K}) = \frac{\sigma_\perp^2}{\sqrt{2\pi}\,\delta_\perp} e^{-\frac{(\vec{K}-K_{0,\perp})^2}{2\delta_\perp^2}} + \frac{\sigma_\parallel^2}{\sqrt{2\pi}\,\delta_\parallel} e^{-\frac{(\vec{K}-K_{0,\parallel})^2}{2\delta_\parallel^2}}. \tag{9}$$

Figure 5(a) displays the anisotropic PSDF that was obtained from the fit to the RAS spectrum recorded following the ion bombardment. Both the positions $K_{0,\perp}$ and $K_{0,\parallel}$, the strengths $\sigma_\perp$ and $\sigma_\parallel$, and the widths $\delta_\perp$ and $\delta_\parallel$ of the two Gaussians were optimized.

Figure 5(b) shows both the measured and fitted RAS spectra at three moments during sputtering, more specifically, after 6, 12, and 18 h. Both the positive and negative features at various

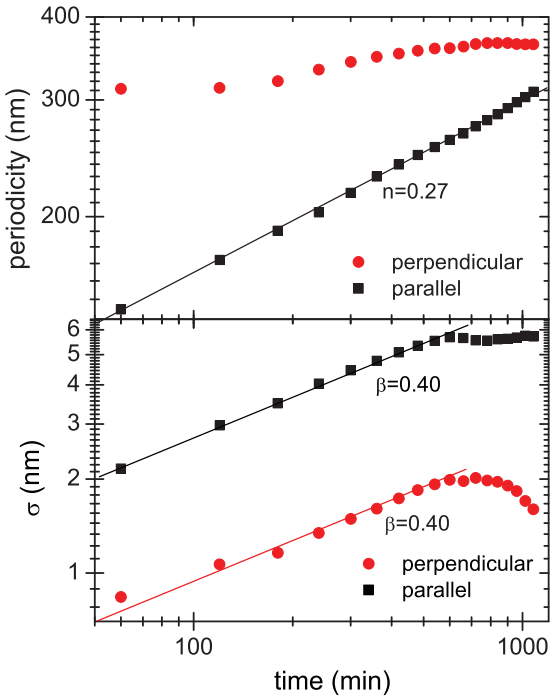

FIG. 6. (Color online) Fit parameters of the RAS spectra obtained during sputtering at a polar angle of incidence of $\theta_i = 61.5°$. (Bottom) Time evolution of the strength of the two Gaussian functions. (Top) Time evolution of the average length scale in the two perpendicular directions.

stages of the ion erosion process are well represented by the PSDF of Eq. (9). For the high photon energy region, above 3.9 eV, the fit is less accurate. At this energy, the silver surface transfers from an excellent mirror in the region before this edge for interband transitions to a strong light absorber. The standard deviation of the RAS signal depends primarily on the reflected intensity.[14] In the fitting procedure, this variation in standard deviation is taken into account, leading to much larger error margins in the high-energy region. Anisotropic strain can be sensitively observed by a fairly sharp feature at ~4 eV.[17,35] Our measurements have not shown any indication of such anisotropic strain induced by oblique incidence ion sputtering.

The periodicity and strength obtained by fitting the spectra recorded during sputtering are displayed in Fig. 6. The temporal evolution of the strength shows a change in behavior at ~580 min. This change is not observed in the evolution of the periodicity in the perpendicular direction. In the initial stage, the perpendicular periodicity is ~200 nm and shows a steady exponential increase with a critical exponent of 0.27. For the entire monitored time window, the periodicity in the parallel direction is well above the periodicity in perpendicular direction. After ~580 min a change in the strength of the periodicity is noted. In the perpendicular direction a saturation is observed, while the periodicity still increases. In the parallel direction the strength even decreases for prolonged sputtering. This signifies that the ordering in this direction becomes smaller and might point to the fact that the surface features become more 1D in this stage.

The evolution of the average periodicity and the strength are often characterized by a critical exponent.[6] The increase of the average periodicity L in the perpendicular direction could be characterized with a critical exponent $n = 0.27$, with $L \propto t^n$. The initial increase of the strength in both directions can be characterized by an exponent β, with $\sigma \propto t^\beta$. For both the perpendicular and parallel directions an almost similar value for β is found, 0.40 ± 0.01. Note however, that in both the periodicity and roughness the exponents only describe the behavior for a limited time window.

VII. CONCLUSION

The optical reflection anisotropy as measured with RAS was used to characterize *in situ* the evolution of the self-organization during oblique incidence ion sputtering of Ag(001). A quantitative analysis of the optical spectra is possible with the Rayleigh-Rice perturbation approach. In this description, the spectra are well represented by two Gaussians representing the anisotropic roughness parallel and perpendicular to the plane of incidence. The temporal evolution of the average periodicity and the roughness amplitude show that the average periodicity between etch features is always larger parallel to the ion beam. Both components grow in a similar way, but after saturation of the anisotropic roughness, the ordering along the beam directions starts to decrease. The combination with LEED measurements show that the induced nanopatterns consist of inverse mounts with a rectangular base.

ACKNOWLEDGMENT

This research is and was supported by NanoNed, a national nanotechnology program coordinated by the Dutch Ministry of Economic Affairs.

[1] R. M. Bradley and J. M. E. Harper, J. Vac. Sci. Technol. A **6**, 2390 (1988).
[2] U. Valbusa, C. Boragno, and F. Buatier de Mongeot, J. Phys. Condens. Matter **14**, 8153 (2002).
[3] M. M. Ovsyanko, Ph.D. thesis, Twente University, 2006.
[4] S. Facsko, T. Dekorsy, C. Koerdt, C. Trappe, H. Kurz, A. Vogt, and H. Hartnagel, Science **285**, 1551 (1999).
[5] T. Aste and U. Valbusa, New J. Phys. **7**, 122 (2005).
[6] Y. Zhao, G.-C. Wang, and T.-M. Lu, in *Experimental Methods in Physical Sciences*, edited by R. Celotta and T. Lucartorto (Academic, New York, 2001), Vol. 37.
[7] C. Boragno, F. Buatier de Mongeot, G. Costantini, U. Valbusa, R. Felici, D.-M. Smilgies, and S. Ferrer, Phys. Rev. B **65**, 153406 (2002).
[8] J. Erlebacher, M. J. Aziz, E. Chason, M. B. Sinclair, and J. A. Floro, Phys. Rev. Lett. **84**, 5800 (2000).
[9] M. B. Chason, E. Sinclair, J. A. Floro, J. A. Hunter, and R. Q. Hwang, Appl. Phys. Lett. **72**, 3276 (1998).
[10] F. Everts, H. Wormeester, and B. Poelsema, Phys. Rev. B **78**, 155419 (2008).
[11] E. Kretschmann and E. Kröger, J. Opt. Soc. Am. **65**, 150 (1975).

[12]H. Raether, in *Tracts in Modern Physics*, edited by G. Höhler (Springer, Berlin, 1988), Vol. 111.
[13]D. E. Aspnes, J. P. Harbison, A. A. Studna, and L. T. Florez, J. Vac. Sci. Technol. A **6**, 1327 (1988).
[14]J.-T. Zettler, K. Haberland, M. Zorn, M. Pristovsek, W. Richter, P. Kurpas, and M. Weyers, J. Cryst. Growth **195**, 151 (1998).
[15]A. Politano and G. Chiarello, J. Phys. D **43** (2010).
[16]P. Weightman, D. S. Martin, R. J. Cole, and T. Farrell, Rep. Prog. Phys. **68**, 1251 (2005).
[17]L. Sun, M. Hohage, P. Zeppenfeld, S. Berkebile, G. Koller, F. Netzer, and M. Ramsey, Appl. Phys. Lett. **12**, 121913 (2006).
[18]N. Witkowski, Y. Borensztein, G. Baudot, V. Repain, Y. Girard, and S. Rousset, Phys. Rev. B **70**, 085408 (2004).
[19]J. M. Flores-Camacho, L. D. Sun, N. Saucedo Zeni, G. Weidlinger, M. Hohage, and P. Zeppenfeld, Phys. Rev. B **78**, 075416 (2008).
[20]J. Flores-Camacho, G. Weidlinger, N. Saucedo Zeni, L. Sun, M. Hohage, and P. Zeppenfeld, Appl. Phys. A **98**, 499 (2010).
[21]D. E. Aspnes, J. B. Theeten, and F. Hottier, Phys. Rev. B **20**, 3292 (1979).
[22]H. Fujiwara, *Spectroscopic Ellipsometry* (Wiley, Hoboken, NJ, 2007).
[23]B. A. Sperling and J. R. Abelson, J. Appl. Phys. **101**, 024915 (2007).
[24]D. Franta and I. Ohlídal, Opt. Commun. **248**, 459 (2005).
[25]S. van Dijken, D. de Bruin, and B. Poelsema, Phys. Rev. Lett. **86**, 4608 (2001).
[26]H. Wormeester and B. Poelsema, J. Phys. Condens. Matter **21**, 224002 (2009).
[27]H. Wormeester, F. Everts, and B. Poelsema, Thin Solid Films **519**, 2664 (2011).
[28]M. Horn-vonHoegen, Z. Kristallogr. **214**, 591 (1999).
[29]L. C. Jorritsma, M. Bijnagte, G. Rosenfeld, and B. Poelsema, Phys. Rev. Lett. **78**, 911 (1997).
[30]H. Niehus, W. Heiland, and E. Taglauer, Surf. Sci. Rep. **17**, 213 (1993).
[31]C. Teichert, C. Ammer, and M. Klaua, Phys. Status Solidi A **146**, 223 (1994).
[32]J. W. Evans, P. A. Thiel, and M. C. Bartelt, Surf. Sci. Rep. **61**, 1 (2006).
[33]F. L. W. Rabbering, H. Wormeester, F. Everts, and B. Poelsema, Phys. Rev. B **79**, 075402 (2009).
[34]F. Everts, H. Wormeester, and B. Poelsema, Phys. Rev. B **82**, 081415(R) (2010).
[35]M. Garfinkel, J. Tiemann, and W. Engeler, Phys. Rev. **148**, 695 (1966).